Deployable Mechanism Design for Span Morphing Wing Aircraft

Chapter · November 2017

DOI: 10.1007/978-981-10-2875-5_66

3 authors, including:

Rongjie Kang
Tianjin University
71 PUBLICATIONS **1,471** CITATIONS

SEE PROFILE

Deployable Mechanism Design for Span Morphing Wing Aircraft

Binbin Gao[1,2], Rongjie Kang[1,2,*] and Yan Chen[1,2] ,

[1] Key Laboratory of Mechanism Theory and Equipment Design of Ministry of Education, Tianjin University, Tianjin 300072, China
[2] School of Mechanical Engineering, Tianjin University, Tianjin 300072, China
{gaobinbin, rjkang, yan_chen}@tju.edu.cn

Abstract. Compared with traditional aircrafts, span morphing wing aircrafts can change their span according to different flight conditions and missions to improve flight performances. Also, it has advantages in storage and transportation. In this paper, a single-degree-of-freedom (SDOF) mechanism based on Sarrus linkages is presented and applied to the construction of a span morphing wing aircraft. Computational Fluid Dynamics (CFD) simulation shows that the deployable mechanism generates slight influence on the drag coefficient while having a relatively strong influence on the lift coefficient and lift to drag ratio. Finite Element Model (FEM) methods are used to analyze the mechanical properties of the mechanism during flight. The results indicate that the maximum stress 45.5 *Mpa* occurs at the link connected to the base link. A series of flight experiments were conducted to prove that the mechanism enables the span change smoothly and improves the flight performances effectively.

Keywords: span morphing wing aircraft, deployable mechanism, computational fluid dynamics simulation, finite element model

1 Introduction

Inspired by nature, people found that birds change their gestures to get a better performance according to different flight conditions. More than 100 years ago, the Wright brothers successfully controlled flight by pulling on cables to twist the wing [1], which brought the first morphing wing aircraft to the world. Morphing wing have attracted great attention among the world since the Defense Advanced Research Projects Agency (DARPA) carried out Morphing Aircraft Structures (MAS) Program between 2002 and 2007 [2, 3, and 4].

Particularly, as a type of morphing wing, span morphing wing can improve the properties of an aircraft and form a multi-role aircraft. The changes of span have

* Corresponding author.
E-mail address: rjkang@tju.edu.cn (R. Kang).

influences on maneuverability, payload, voyage and specific fuel consumption of an aircraft. In consideration of economy, using one multi-role span morphing wing aircraft to replace several types of aircrafts tailored for specific missions saves production cost largely. Also, it brings benefits to the storage and transportation of the aircraft [4, 5].

The first span morphing wing concept was presented by an American aircraft designer named Vincent in1929 and in the same year, he designed and manufactured a morphing aircraft GX-3 which could change its span and camber simultaneously [6]. Previous researches on span morphing wing included telescoping wing aircraft [7, 8], the Lockheed Martin's Z-wing concept [9, 10], the modular variable geometry truss mechanism configuration [11, 12] and so on. Most of the above concepts require multi-degree-of-freedom (MDOF) movement, in other words, more than one actuators are needed to achieve wing morphing. For the Lockheed Martin's Z-wing concept, the span morphing wing consists of an inner panel and an outboard panel. The span changes by folding the inner panel to the fuselage. There are two actuators in the leading edge flap, one actuator between the inner panel and fuselage while the other one between the inner panel and outboard panel. For the modular variable geometry truss mechanism configuration, eight actuators were used to control each module, as the number of modules increases, the number of actuators increases accordingly. The use of a large numbers of actuators will decrease payload, increase specific fuel consumption, narrow voyage, bring a complex control system to an aircraft. Additionally, the rigidities of MDOF mechanisms are usually insufficient, which means unexpected deformations may occur in the wing structure. To solve the above problems, a single-degree-of-freedom (SDOF) mechanism is required for span morphing wing aircraft.

Traditional SDOF mechanisms for span morphing wing aircraft include screw rod and guide rail, gear and rack, the scissor mechanism configuration. Chen et. al [13] presented a span morphing wing aircraft driven by screw rod and guide rail. The active wing is attached to a slider on the guide rail. The rotation of the screw rod causes the slider to translate which enables the active wing to move relatively to the fixed wing. The screw rod and guide rail mechanism can change the span accurately. However, there are slight deformations at the wing that may cause issues on the relative displacements between the screw rod and the nut, the guide rail and the slider, even making the slider stuck. In 2005, Alemayehu et. al [14] designed a span morphing wing aircraft based on the gear and rack mechanism. The active wing is attached to the rack. This design can make the active wing translate smoothly, efficiently and reliably. But large space is needed to install the mechanism in the direction perpendicular to the wing surface and the length of the span is restricted by the size of the rack. Wu et. al [15] changed the span by the scissor mechanism which consists of scissor units assembled in series. This design is simple and reliable, and the driving force is small. However, the rigidity of the mechanism will decrease greatly if the number of units increases.

In 2012, Wang et. al [16] presented a novel design based on a SDOF overconstrained mechanism, the Sarrus linkage, for span-changing aircrafts. The outboard wing was attached to one end of the deployable mechanism, and the other end of the mechanism was fixed to the inner wing. The mechanism was driven by a servo and the span of aircraft can change form minimum $1.43\,m$ to maximum

1.77 m . The reference area changes 23.5% accordingly. The space required for installation is small and the mechanism is of high folding ratio. As each links are connected by revolute joints, the driving moment is small. Since the mechanism is overconstrained, the morphing wing is of high rigidity.

However, many problems were found through later flight tests. Firstly, the connection between the mechanism and the inner wing is not firm, where deformations were easy to take place. Secondly, the folding ratio for the span (23.5%) is not large enough. Thirdly, as the outboard wing takes more load, the driving moment for the mechanism increases greatly. To solve the above problems, a new generation of span morphing wing aircraft is designed and manufactured in this paper. To decrease the deformation in the connection, a specific connecter is designed to connect the inner wing and deployable mechanism. To improve the changing ratio of reference area to 50%, which is a standard for span morphing wing aircraft [17], the number of the Sarrus units in the deployable mechanism triples. To reduce the driving moment for the mechanism, rolling bearings are applied to all revolute joints.

This paper is organized as follows: Section 2 and 3 presents the design and simulated analysis of the morphing wing using Sarrus linkages, respectively; a series of experiments are then carried out to test the performance of the span morphing wing aircraft in Section 4; and the conclusions are given in Section 5.

2 Morphing Wing Mechanism Design

The new morphing wing aircraft is based on a multi-segmented Sarrus linkages. As shown in Fig. 1, this mechanism consists of four parallelogram units connected by three Sarrus linkages.

In this mechanism, the links w, k_1, s_1, k_2, s_2, k_3, s_3, r have the same length,

$$l_w = l_{k_1} = l_{s_1} = l_{k_2} = l_{s_2} = l_{k_3} = l_{s_3} = l_r = \delta \tag{1}$$

Also, the links p_1, q_1, p_2, q_2, p_3, q_3, p_4, q_4 have the same length,

$$l_{p_1} = l_{q_1} = l_{p_2} = l_{q_2} = l_{p_3} = l_{q_3} = l_{p_4} = l_{q_4} = l \tag{2}$$

The unit T_1 formed by w, p_1, k_1, q_1 and T_4 formed by r, p_4, s_3, q_4 are identical, the unit T_2 formed by s_1, p_2, k_2, q_2 and T_3 formed by s_2, p_3, k_3, q_3 are the same. Two units T_1 and T_2 are connected by linking p_1, p_2 and q_1, q_2 respectively with two revolute joints. The links k_1 and s_1 are connected to two identical the links m_1 and n_1 by a revolute joint, respectively. The other ends of links m_1 and n_1 are connected to each other by a revolute joint. The first Sarrus linkage consists of the links p_1, k_1, m_1, p_2, s_1, n_1, so the mechanism formed by the units T_1 and T_2 is SDOF. Rotating the link p_1 around the link w can make the link k_2 translate in the direction perpendicular to link w. In the same way, the units T_2 and T_3, T_3 and T_4 are connected by the Sarrus linkages, so the deployable mechanism is SDOF, the mechanism can be extended by rotating any link in it.

According to equations (**1**) and (**2**), the mechanism becomes symmetrical about the middle line that connects the p_2- p_3 joint and the q_2- q_3 joint. In the mechanism, the

rotational motion of link p_1 would result in the linear motion of link r, and the direction of this linear motion is always perpendicular to the link w, link w is connected to the inner wing by a specific connecter and the outboard wing is fixed to the link r.

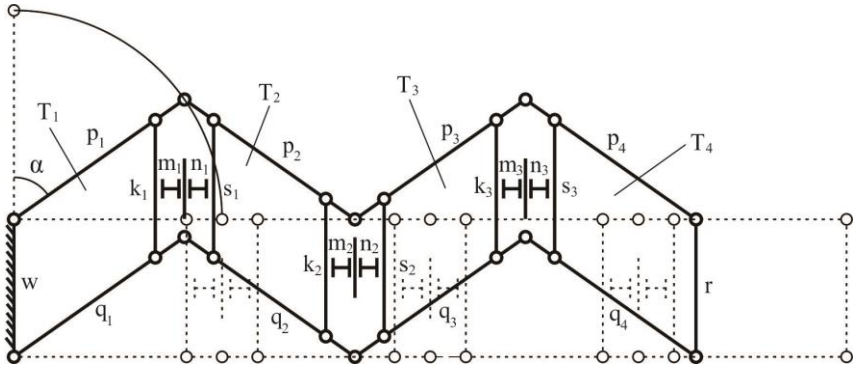

Fig. 1. Schematic of the span morphing wing mechanism

Define α as the driving angle between the links p_1 and w, t as the thickness of the links w, r, and D as the instantaneous displacement of r from w, when p_1 is driven around the revolute joint between w and p_1. Due to the symmetry of the mechanism with respect to the middle line, it can be found that

$$D = 4l\sin\alpha + 2t \tag{3}$$

Taking the derivative of (3), the velocity of link r is

$$V = \frac{dD}{d\alpha} = 4l\cos\alpha \tag{4}$$

In equations (**3**) and (**4**) the driving angle α is between 0^o and 90^o.

A three-dimensional model is created in SOLIDWORKS 2014, where $\delta = 0.055\ m$, $l = 0.085\ m$, $t = 0.004\ m$. To improve the strength and reduce the weight of the deployable structure, the links p_1, q_1, p_2, q_2, p_3, q_3, p_4, q_4 are designed to be an I-shape beam. Besides, unnecessary supports are removed from all links. All the sharp corners of the links are rounded in order to avoid possible stress concentrations. The extension process of the mechanism is shown in Fig. 2. The rotation angle α for the four gestures correspond to 0^o, 30^o, 60^o, 90^o.

When the mechanism fully extends, the maximum displacement D_{max} is $0.34\ m$. When the mechanism fully folds, as shown in Fig. 2-a, there are seven revolute joints placed one by one along the extending direction. Every joint has a size of $0.008\ m$, so the minimum displacement D_{max} is $0.056\ m$. This mechanism is designed to be attached to a prototyped aircraft with a reference area A_0 of $0.27\ m^2$ and chord length C of $0.257\ m$. The instantaneous reference area A can be calculated by

$$A = A_0 + 2DC \tag{5}$$

When the mechanism fully folds, it can be found that

$$A_{min} = A_0 + 2D_{min}C \approx 0.2988\ m^2 \tag{6}$$

When the mechanism fully extends, it can be found that

$$A_{max} = A_0 + 2D_{max}C \approx 0.4489\ m^2 \tag{7}$$

Thus, the reference area changing ratio is

$$\psi = \frac{A_{max} - A_{min}}{A_{min}} = 0.5023 \tag{8}$$

The maximum reference area changing ratio for the span morphing aircraft is 50.23%, which is larger than 50%.

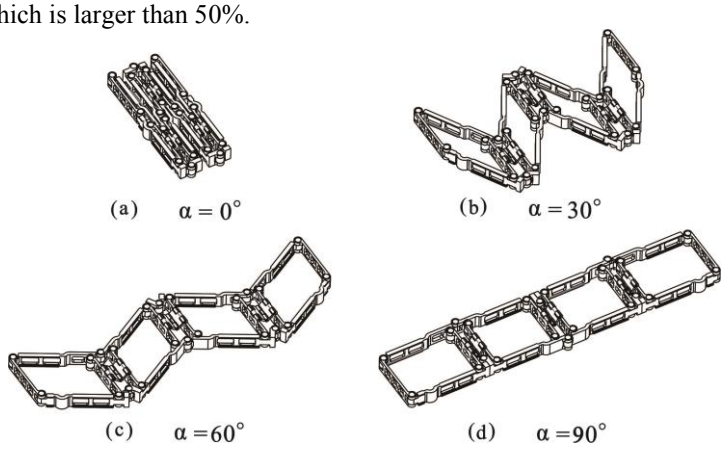

Fig. 2. Extension process of the deployable mechanism.

Figure 3 shows the prototype of the span morphing wing aircraft. To illustrate the deployable mechanism clearly, the covering skin is removed. During real flights, rigid skin is attached to the inner wing. The section shape of the rigid skin is the same as the outboard wing and the section size of the rigid skin is a little bit larger than the outboard wing to ensure the smooth movement and the adequate lift.

3 Simulations and Analyses

The CFD simulations were carried out to study the aerodynamic performances of the span morphing wing. Since the payload, the maneuverability and the voyage of an aircraft are highly affected by the wing parameters, such as the lift coefficients, the drag coefficients and the lift to drag ratios, it is necessary to change the wing span to optimize these parameters according to the flight conditions and missions. Above parameters are also related to the angle of attack (AOA), so the changes of the

parameters with respect to different AOA need to be compared. The FEM analyses were then used to locate the maximum stresses and to improve the design of the deployable mecchanism.

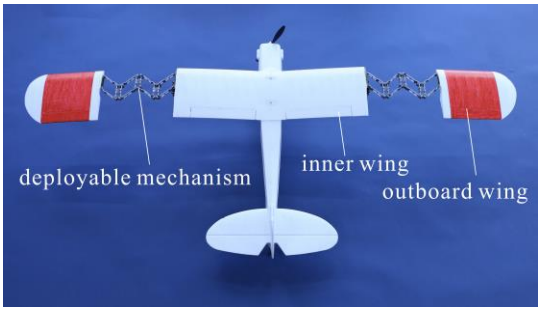

Fig. 3. The prototyped airplane with morphing wing mechanism installed

3.1 Computational Fluid Dynamics Simulations

Seven models with the driving angles of 0^o, 10^o, 20^o, 30^o, 40^o, 60^o, 90^o are set up in CATIA V5, and then these models are put into GAMBIT for meshing. In the end, these models are imported into FLUENT, a plug-in from ANSYS 15.0, which is used for CFD simulation. In simulations, the Spalart-Allmaras (SA) model is chosen to set up the turbulence model. Assuming that the flight tests are carried out at sea level and the air temperature is 288.15 kelvins, the designed air speed is $U = 12\ m/s$, the air density is $\rho = 1.225\ kg/m^3$, the air viscosity is $\mu = 1.789 \times 10^{-5}\ pa \cdot s$. The Reynolds number can be obtained by

$$Re = \frac{\rho UC}{\mu} = 2.11 \times 10^5 \tag{9}$$

Figure 4 shows that for a certain model, when the AOA increases, both the lift coefficient and the drag coefficient get larger. The lift coefficient curves approximate a straight line while the drag coefficient curves approximate a quadratic curve.

On the other hand, for the same AOA, the increasing span result in growing lift coefficients, though the growth are small. Table 1 presents the changes of the lift coefficients in percentage relative to the folding condition. As the AOA gets larger, the percent changes get smaller.

Though the lift coefficient changes very small, the lift force increases greatly as span gets larger.

$$F_L = \frac{1}{2} C_L A \rho U^2 \tag{10}$$

where F_L is the lift force and C_L stands for the lift coefficient, based on other parameters being hold, 50% increase in the reference area A will result in at least 50%

increase in the lift force. Combining equations (**5**) and (**10**), it indicates that, there is a linear relationship between lift force F_L and D , as shown in equation (**11**).

$$F_L = \frac{1}{2} C_L (A_0 + 2DC)\ \rho U^2 \tag{11}$$

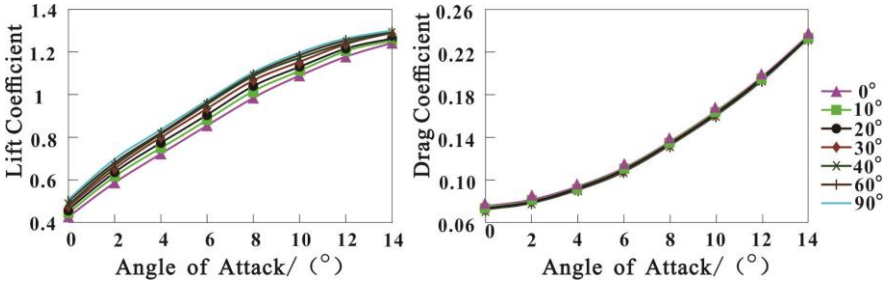

(a) (b)

Fig. 4. Relationship between (a) the lift coefficients and the angles of attack, (b) the drag coefficients and the angles of attack.

Table 1. Percentage changes in the lift coefficients under different spans

Changes of Lift Coefficients (%)	Degree of expansion (º)					
AOA (º)	10	20	30	40	60	90
0	3.3	6.2	8.8	10.6	13.7	15.0
2	4.2	6.7	8.8	11.0	12.9	14.0
4	2.8	5.6	8.7	10.0	10.3	12.0
6	2.6	4.8	7.5	9.7	10.5	11.5
8	2.4	4.4	6.5	8.0	8.8	9.3
10	1.4	2.8	4.6	6.2	7.1	8.2
12	2.0	2.7	4.0	4.3	5.2	5.8
14	0.06	1.3	3.0	3.1	3.4	3.7

Unlike the lift coefficients, as shown in Table 2, the drag coefficients for a constant AOA decreases slowly when the mechanism extends. In conclusion, airfoil shape rather than span morphing, dominates the values of the lift and drag coefficients.

Using the drag coefficient C_D to replace the lift coefficient C_L in equation (**10**), the ideal drag force F_D is

$$F_D = \frac{1}{2} C_D A \rho U^2 \tag{12}$$

Combining equations (**5**) and (**12**), as shown in equation (**13**), above linear relationship can be applied to drag force F_D and D as

$$F_D = \frac{1}{2} C_D (A_0 + 2DC) \ \rho U^2 \tag{13}$$

Table 2. Percentage changes in the drag coefficients under different spans

Changes of Drag Coefficients (%)	Degree of expansion (^{o})					
AOA (^{o})	10	20	30	40	60	90
0	-2.1	-4.7	-4.7	-5.4	-5.6	-5.8
2	-3.1	-4.5	-4.6	-4.7	-4.7	-6.2
4	-2.0	-2.5	-3.1	-4.6	-4.8	-5.0
6	-1.2	-2.6	-3.7	-4.1	-4.4	-5.1
8	-1.0	-2.2	-2.5	-2.9	-2.9	-3.9
10	-0.8	-2.6	-3.2	-3.3	-3.5	-3.7
12	-1.0	-1.1	-1.6	-1.7	-2.5	-3.4
14	-0.5	-0.8	-1.0	-1.2	-1.4	-1.6

Figure 5 shows that, for a certain span, the lift to drag ratio increases first and then decreases, as the AOA increases. Though the changes of the lift coefficients and drag coefficients change slightly when the mechanism extends, there is a significant increase in the lift to drag ratio L/D. The maximum L/D 9.15 occurs when AOA is closed to 5^o and the mechanism fully extends.

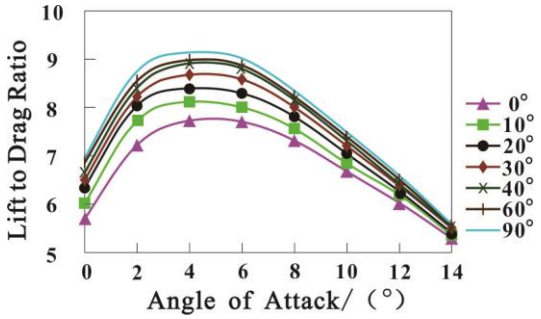

Fig. 5. Relationship between the lift to drag ratios and the angles of attack

Table 3 shows the details of the changes. It indicates that, the influence of the span morphing on the lift to drag ratio gets less as the AOA increases.

Table 3. Percentage changes in the lift to drag ratios under different spans

Changes of L/D (%)	Degree of expansion (^{o})					
AOA (^{o})	10	20	30	40	60	90
0	5.5	11.3	14.2	16.9	20.5	22.1
2	7.5	11.8	14.0	16.5	18.5	21.5
4	4.9	8.2	12.1	15.3	16.0	17.8
6	3.8	7.6	11.6	14.4	15.5	17.4
8	3.5	6.7	9.2	11.1	12.0	13.8
10	2.2	5.6	8.0	9.8	11.0	12.3
12	3.1	3.9	5.7	6.0	7.9	9.4
14	1.1	2.1	4.0	4.4	4.9	5.4

3.2 Finite Element Model Analyses

From CFD simulations, the lift coefficient and the drag coefficient for each model under different AOA have been obtained. Combining (11) and (13), the lift and drag forces are derived. In this section, 10 models are built with the driving angles of $0^o, 10^o, 20^o, 30^o, 40^o, 50^o, 60^o, 70^o, 80^o, 90^o$. They are meshed in fore treatment software HYPERMESH. FEM analyses are carried out on morphing mechanism to find the maximum stresses and locating their positions with commercial finite element method (FEM) software ABAQUS 6.13. Assuming the aluminum T6061 is used to fabricate the morphing mechanism. For the boundary conditions, the lift force, drag force as well as the gravity are applied to the wing surface, and a fixed support is applied at the wing root. The driving link on the mechanism is set to have no rotation.

Figure 6 shows the changes of the maximum stresses for 10 models under different AOA. Ignoring several points with large deviation, the maximum stresses increases as AOA get larger. In other words, the increasing AOA results in a rapid growth of lift force and drag force, which causes a large deformation in the mechanism. However, for a constant AOA, as the mechanism extends, the maximum stresses increases first and then decreases. The peak point occurs when the driving link angle is around 50^o. The reason may be that a mechanical disadvantage occurs when the driving angle chose to 50^o.

All maximum stresses occur at the link next to the base link, which is the thinnest part of the linkage, as shown in Fig. 7. The whole mechanism can be considered as a cantilever beam. The largest value among all maximum stresses is $45.5\ Mpa$ when the mechanism has an extension of 50^o and the AOA is 14^o. It indicates that,

Aluminum T6061 with a yielding stress $275\,Mpa$ is safe enough for the prototype of the span morphing wing aircraft.

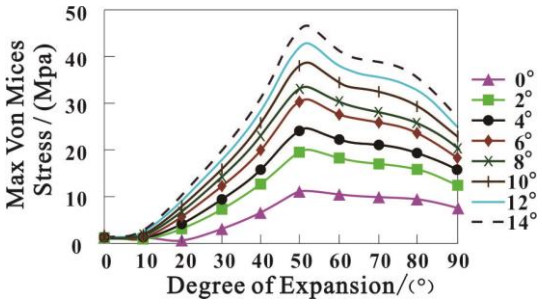

Fig. 6. Relationship between the maximum stresses and the driving angles.

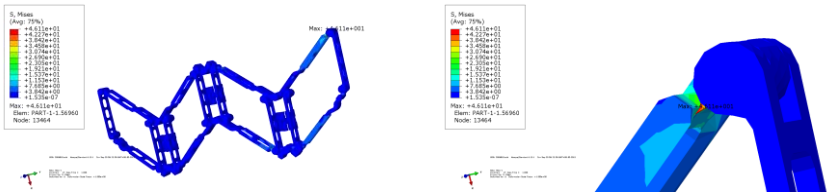

(a) (b)

Fig. 7. The maximum stress observed in the structure with 50° deflection under 14° angle of attack: (a) overall view of the stress distribution in the mechanism; (b) zoomed view of the position of where the maximum stress occurred.

4 Flight Performance

To assess the performances of the span morphing prototyped plane after refitted, a series of experiments were conducted under similar wind condition. A micro-camera is affixed to a rigid portion of the fuselage and directed towards the morphing wing to record the movement of the wing. Figure 8 shows the flight tests.

The experiments were carried out with the driving angles of 0^o, 30^o, 90^o, which correspond to the dash configuration, the intermediate configuration, the loiter configuration [10], and focus on the performances of takeoff distance, stability and maneuverability. The takeoff distances are measured under different configurations with full throttle and maximum elevator deflection. The results show that the loiter configuration needs a takeoff distance within $10\,m$ to take off and the dash configuration needs more than $15\,m$. The stability includes flight stability and landing stability. Experiments show that the loiter configuration has better stability than the other two configurations. A mutational wind condition brings more risk to the dash configuration during flight. The loiter configuration allows for an easier landing. Though the loiter configuration has worse stability, it has better maneuverability.

When the plane needs to turn around, the turning radius of the dash configuration is much smaller. For the same thrust, the dash configuration has a larger speed and acceleration than other two configurations.

The voyage, the maneuverability and the load weight of the plane improve a lot after applying the deployable mechanism to the wing. However, there are also limitations of the plane. Its deadweight increases from $0.85\,Kg$ to $1.5\,Kg$ i.e. its inertia increases and its maneuverability gets worse.

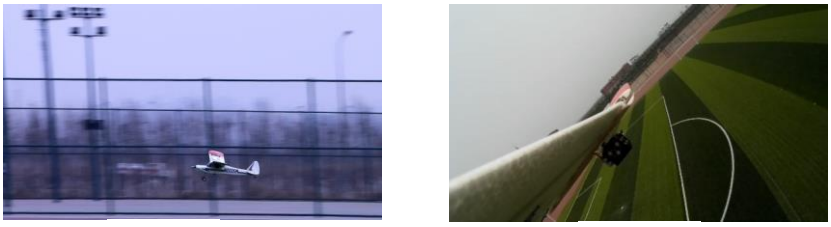

(a) (b)

Fig. 8. Photos for flight performance tests: (a) video snapshot from the ground; (b) video snapshot from the on-board camera.

5 Conclusion and Discussion

In this paper, a deployable mechanism based on the Sarrus linkages is presented to construct a span morphing wing aircraft. The design of the mechanism is investigated with a brief kinematics analyses. To analyze the influence of span morphing on aerodynamic performances of the prototyped aircraft, CFD simulations were carried out. FEM analyses were used to help to select the appropriate material for the deployable mechanism. And a series of experiments were then conducted to test the design.

It was found that the changes of span have slight influences on the lift coefficient and the drag coefficient while can improve the lift force and drag force by 50%. It proves that the mechanism is able to inprove the aerodynamic performance of a span morphing wing aircraft.

The maximum stress occurs when the mechanism is semi-expanded. The yielding stress of the selected material Aluminum T6061 is much larger than the maximum stress $45.5\,Mpa$, which indicates that material is safe enough in the span morphing wing aircraft.

In the future, small sensors and data acquisition devices will be used to measure and record the command input and aircraft response during flight. In that case, the performance of the span morphing wing aircraft can be parameterized. Also, the weight of the plane must be reduced to decrease its inertia and improve its maneuverability. Then the rigidity of the wing needs to be enhanced to reduce deformations in the outboard wing and improve the performances of the span morphing wing aircraft.

Acknowledgements

The authors acknowledge the supports of the National Natural Science Foundation of China (Project No. 51275334 and 51375329).

References

1. Bowman, J., Sanders, B., Cannon, B.: Development of next generation morphing aircraft structures. In: 48th AIAA/ASME/ASCE/AHS/ASC Structures, Structural Dynamics, and Materials Conference, 1730. AIAA Press, Honolulu (2007)
2. Love, M.H., Zink, P.S., Stroud, R.L.: Demonstration of morphing technology through ground and wind tunnel tests. In: 48th AIAA/ASME/ASCE/AHS/ASC Structures, Structural Dynamics, and Materials Conference, 1729. AIAA Press, Honolulu (2007)
3. Weisshaar, T.A.: Morphing aircraft systems: history perspectives and future challenges. Journal of Aircraft, vol. 50(2), pp. 337--353 (2013)
4. Rodriguez, A.R.: Morphing aircraft technology survey. In: 45th AIAA Aerospace Sciences Meeting and Exhibit, 1258. AIAA Press, Reno (2007)
5. Bowman, J., Sanders, B., Weisshaar, T.A.: Evaluating the impact of morphing technologies on aircraft performance. In 43rd AIAA/ASME/ASCE/AHS/ASC Structures, Structural Dynamics, and Materials Conference, 1631. AIAA Press, Denver (2002)
6. Rodriguez, A.R.: The contributions of Vincent Justus Burnelli. In: 41st AIAA Aerospace Sciences Meeting and Exhibit, 292. AIAA Press, Reno (2002)
7. Blondeau, J., Pines, D.J.: Design development and testing of a morphing aspect ratio wing using an inflatable telescopic spar. In: 44th AIAA/ASME/ASCE/AHS/ASC Structures, Structural Dynamics, and Materials Conference, AIAA Press, Norfolk (2003)
8. Neal, D.A., Johnston, C.O.: Design and wind-tunnel analysis of a fully adaptive aircraft configuration. In: 45th AIAA/ASME/ASCE/AHS/ASC Structures, Structural Dynamics, and Materials Conference, AIAA Press, California (2004)
9. Baldelli, D.H., Lee, D.H., Hopper, D.: Practical modeling, control and simulation of an aeroelastic morphing UAV. In: 48th AIAA/ASME/ASCE/AHS/ASC Structures, Structural Dynamics, and Materials Conference, 2236. AIAA Press, Honolulu (2007)
10. Ivanco, T.G., Scott, R.C., Love, M.H.: Validation of the Lockheed martin morphing concept with wind tunnel testing. In: 48th AIAA/ASME/ASCE/AHS/ASC Structures, Structural Dynamics, and Materials Conference, 2235. AIAA Press, Honolulu (2007)
11. Moosavian, A., Xi, F.F., Hashemi, S.M.: Design and motion control of fully variable morphing wings. Journal of Aircraft, vol. 50(4), pp. 1189--1201 (2013)
12. Moosavian, A., Xi, F.F., Hashemi, S.M.: Optimal configuration design for the variable geometry wing-box. Journal of Aircraft, vol. 51(3), pp. 811--823 (2014)
13. Chen, X.: Design of an axially telescoping wing control system and nonlinear vibration experiment research, Beijing University of Technology, Beijing, China (2012)
14. Alemayehu, D., Leng, M., Mcnulty, R.: Virginia Tech morphing wing team spring 2005 final report (2005)
15. Wang, L.J.: The scheme design of the UAV morphing wing and simulation analysis, Harbin Institute of Technology, Harbin, China (2014)
16. Wang, Q., Chen, Y., Tang, H.: Mechanism design for aircraft morphing wing. In 53rd AIAA/ASME/ASCE/AHS/ASC Structures, Structural Dynamics, and Materials Conference, 1608. AIAA Press, Honolulu (2012)
17. Ramrakhyani, D.S., Lesieutre, G.A., Frecker, M.: Aircraft structural morphing using tendon-actuated compliant cellular trusses. Journal of Aircraft, vol. 52(6), pp. 1615--1621 (2005)